Natural Resources Canada
Ressources naturelles Canada

Sedimentary architecture of a deeply karsted Precambrian–Cambrian unconformity, Victoria Island, Northwest Territories

J. Mathieu, E.C. Turner, and R.H. Rainbird

Geological Survey of Canada
Current Research 2013-1

2013

Canada

Geological Survey of Canada
Current Research 2013-1

Sedimentary architecture of a deeply karsted Precambrian–Cambrian unconformity, Victoria Island, Northwest Territories

J. Mathieu, E.C. Turner, and R.H. Rainbird

2013

ISSN 1701-4387
Catalogue No. M44-2013/1E-PDF
ISBN 978-1-100-21516-7
doi:10.40956/292099

A copy of this publication is also available for reference in depository libraries across Canada through access to the Depository Services Program's Web site at http://dsp-psd.pwgsc.gc.ca

This publication is available for free download through GEOSCAN
http://geoscan.ess.nrcan.gc.ca

Recommended citation

Mathieu, J., Turner, E.C., and Rainbird, R.H., 2013. Sedimentary architecture of a deeply karsted Precambrian–Cambrian unconformity, Victoria Island, Northwest Territories; Geological Survey of Canada, Current Research 2013-1, 15 p. doi:10.4095/292099

Critical review
K. Dewing
T. Hadlari

Authors

J. Mathieu (jy_mathieu@laurentian.ca)
E.C. Turner (eturner@laurentian.ca)
Department of Earth Sciences
Laurentian University
935 Ramsey Lake Road
Sudbury, Ontario
P3E 2C6

R.H. Rainbird (Rob.Rainbird@NRCan-RNCan.gc.ca)
Geological Survey of Canada
601 Booth Street
Ottawa, Ontario
K1A 0E8

Correction date:

Sedimentary architecture of a deeply karsted Precambrian–Cambrian unconformity, Victoria Island, Northwest Territories

J. Mathieu, E.C. Turner, and R.H. Rainbird

Mathieu, J., Turner, E.C., and Rainbird, R.H., 2013. Sedimentary architecture of a deeply karsted Precambrian–Cambrian unconformity, Victoria Island, Northwest Territories; Geological Survey of Canada, Current Research 2013-1, 15 p. doi:10.4095/292099

Abstract: A deeply karsted unconformity separates Proterozoic carbonate rocks of the Wynniatt Formation from overlying Cambrian sandstone near the head of Minto Inlet on Victoria Island, Arctic Canada. Sandstone-filled paleocaverns, hundreds of metres wide and tens of metres high, are present approximately 10 to 15 m stratigraphically below the nominal stratigraphic contact between Proterozoic and Cambrian rocks; the position of the paleocaves relative to the main unconformity surface suggests development along a paleointerface possibly associated with the water table. Gryke networks and karstic towers are present in the Wynniatt Formation at the unconformity. Crossbedded sandstone that overlies the unconformity contains unusual, vertical columnar sandstone structures, decimetres to metres in diameter, which cut sharply across bedding and contain weak concentric layering. These pillar-like structures are attributed to water escape through submarine springs, where groundwater flowing through the karst network emerged onto the Cambrian seafloor. The pillars are most densely clustered in the most northern exposure of the sandstone, and diminish in abundance southward, suggesting that the coastline and the source of hydraulic head were to the north of the study area.

Résumé : Près du fond de l'inlet Minto, sur l'île Victoria (Arctique canadien), une discordance profondément karstifiée sépare les roches carbonatées protérozoïques de la Formation de Wynniatt du grès cambrien sus-jacent. Des paléocavernes remplies de grès, mesurant des centaines de mètres de largeur et des dizaines de mètres de hauteur, sont situées stratigraphiquement environ 10 à 15 m sous le contact stratigraphique nominal entre les roches du Protérozoïque et du Cambrien; la position relative des paléocavernes par rapport à la surface de discordance principale laisse supposer un développement le long d'une paléointerface vraisemblablement associée à la surface de la nappe d'eau souterraine. Des réseaux de lapiés (fentes de dissolution) et des tours karstiques sont présents dans la Formation de Wynniatt tout près de la discordance. Le grès à stratification oblique qui surmonte la discordance contient des structures de grès columnaires verticales inusitées, de plusieurs décimètres à plusieurs mètres de diamètre, qui recoupent nettement le litage et présentent une faible stratification concentrique. Ces structures en forme de piliers sont attribuées à l'écoulement d'eau par des sources sous-marines, là où les eaux souterraines circulant à travers le réseau karstique émergeaient sur le fond marin du Cambrien. Les piliers sont plus densément groupés dans la partie la plus septentrionale de l'affleurement de grès, tandis que leur nombre diminue vers le sud, ce qui donne à penser que le rivage et la source de la charge hydraulique se situaient au nord de la zone d'étude.

INTRODUCTION

Victoria Island (Fig. 1) is underlain by strata of the Neoproterozoic Shaler Supergroup and poorly known, informally defined Cambrian to Devonian sedimentary units dominated by carbonate rocks and subordinate quartzose sandstone. The two successions are separated by a hiatus of approximately 200 Ma.

The unconformity between Proterozoic and lower Paleozoic strata locally cuts down to the level of the Wynniatt Formation. This implies removal of 1 to 2 km of strata. The unconformity is locally well exposed and preserves clear evidence of deep karstification. The focus of this project is to document these karst-related features present in the Wynniatt Formation and their effect on deposition of overlying Cambrian sandstone.

REGIONAL GEOLOGY

The bedrock geology of Victoria Island is divided into two main regions (Fig. 1): a central core of weakly metamorphosed and broadly folded Neoproterozoic strata, known as the Minto Inlier, and large flanking areas underlain by poorly exposed, mainly flat-lying, largely undescribed Paleozoic rocks. The geology of Victoria Island was first described by Washburn (1947) in a report that dealt mainly with glaciation and geomorphology. A more comprehensive description of the bedrock geology, including definition of Proterozoic sedimentary rocks of the Shaler Group and a 1:1 000 000 geological map, was produced by Thorsteinsson and Tozer (1962). The Shaler Group was studied in more detail by Young (*see* Young, 1981 and references therein) and then by Rainbird (e.g. Rainbird, 1991, 1992a), who further subdivided the stratigraphy and elevated the Shaler Group to Supergroup (Rainbird et al., 1994). The Shaler Supergroup consists of the Rae Group (previously the Glenelg Formation of Thorsteinsson and Tozer, 1962), the Reynolds Point Group, and the Minto Inlet, Wynniatt, Kilian, Kuujjua, and Natkusiak formations.

The Wynniatt Formation is a succession of shallow-marine limestone and dolostone that was divided into four informal members (Rainbird, 1991): the 'lower', 'shale', 'stromatolitic', and 'upper' members. The Kilian Formation consists of evaporite rocks interlayered with shale, sandstone, and limestone, and was divided into eight informal members that form three complete upward-shallowing sequences. The Kuujjua Formation consists mainly of coarse-grained quartz arenite that was deposited in a broad fluvial braid plain (Rainbird, 1992a). The uppermost unit of the Shaler Supergroup is the Natkusiak Formation, a 1100 m thick flood basalt that is part of the Franklin igneous event (ca. 720 Ma; Heaman et al., 1992). Two regional folds affect the Proterozoic succession on Victoria Island: the northeast-trending Walker Bay anticline and Holman Island syncline. Neither of these folds causes inclination of strata to exceed 10°. Phanerozoic strata are not affected by these folds (Thorsteinsson and Tozer, 1962).

The Shaler Supergroup is considered to be of early Neoproterozoic age based on detrital zircon geochronology (Rainbird et al., 1992, 1997) and has been correlated with the Mackenzie Mountains supergroup (Rainbird, 1992b; Rainbird et al., 1996, 1997; Long et al., 2008; Jones et al., 2010). The Shaler Supergroup is unconformably overlain by Phanerozoic strata including Cambrian to Silurian rocks (based on fossil assemblages) mapped as units 10a and 10b by Thorsteinsson and Tozer (1962). Map unit 10a, the basal unit, was described as sandstone with dolostone and shale. Map unit 10b was described as a fairly uniform succession of Ordovician to Silurian dolostone and is the most common bedrock type on the island.

METHODS

An area of approximately 1.5 km^2 was mapped near the head of the Minto Inlet (Fig. 1) where the karsted unconformity is exposed. This area represents a site in which 1 to 2 km of subaerial erosion occurred prior to the preservation of the paleokarst by burial under younger strata. Collection of geographic co-ordinates for all exposed karst and cylindrical sandstone structures was achieved using a portable computer/GPS (Getac) unit. Accuracy of the GPS co-ordinates was within a few metres.

RESULTS

The detailed map region contains exposures of the 'upper carbonate member' of the Wynniatt Formation in the north, and the 'lower clastic' and 'tan' Cambrian units (map unit 10a of Thorsteinsson and Tozer (1962)) toward the south (Fig. 2). It should be noted that within the mapped area there are several areas of Quaternary cover. The contact between Proterozoic and Paleozoic units trends northeast. Strata of the Wynniatt Formation are subhorizontal, and Paleozoic strata are almost flat-lying; the land surface rises to the southeast such that progressively younger Proterozoic strata are preserved.

Wynniatt Formation

The upper carbonate member of the Wynniatt Formation in the study area is a pale tan- to grey-weathering dolostone, made up of fine to medium-sized crystals, that is thickly laminated to medium-bedded at a centimetre to decimetre scale (Fig. 3a). Bedding dips 5 to 7° to the southeast. Along the north edge of the mapped area, the dolostone is pale grey and has wavy laminations and thin bedding. Molar-tooth structure, intraclasts, zebra dolomite (Fig. 3b), chert nodules

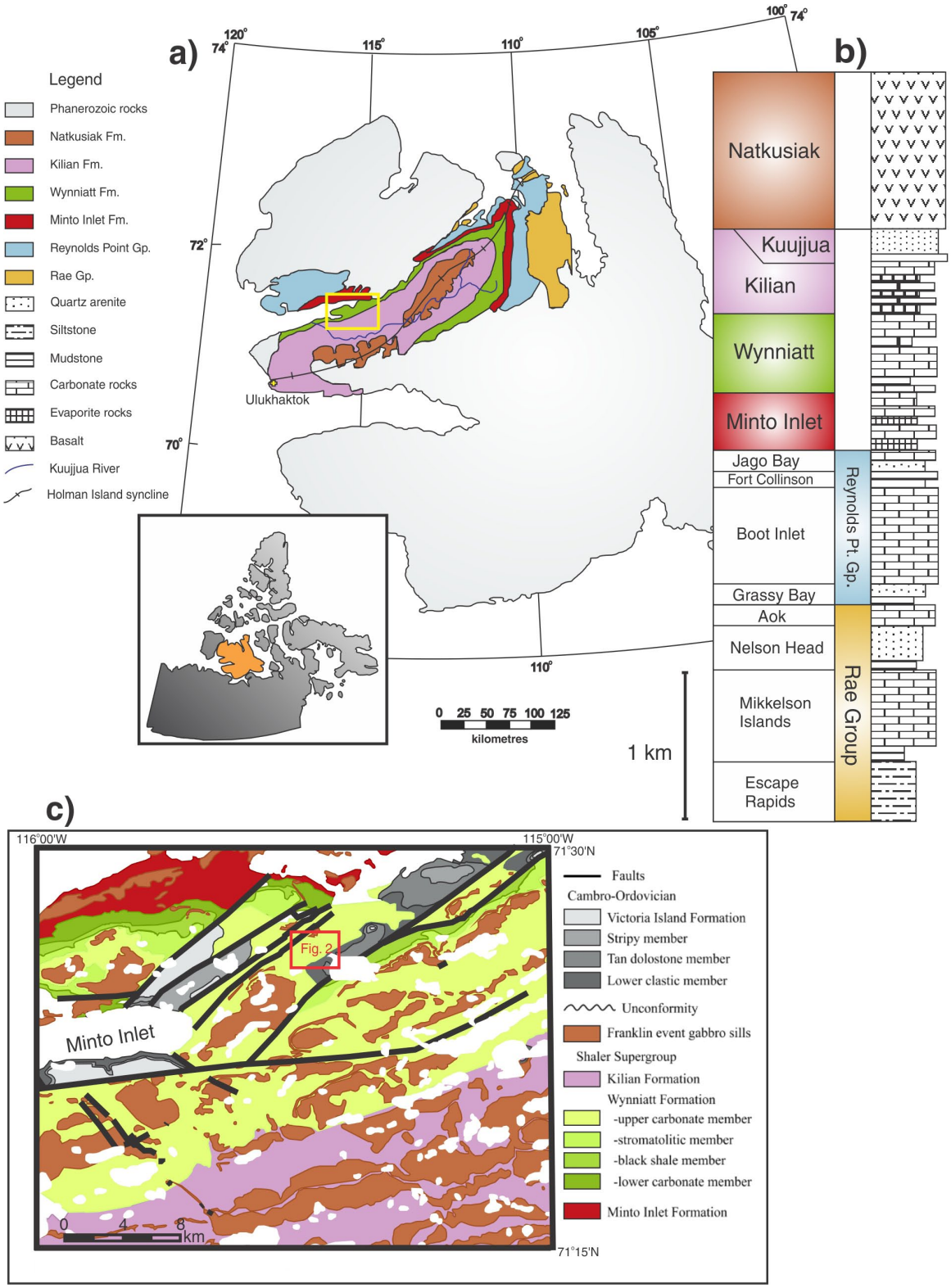

Figure 1. a) Bedrock geology of Victoria Island (*after* Thorsteinsson and Tozer, 1962, Map 1135A [in pocket]), highlighting the Minto Inlier (coloured). Inset shows location of Victoria Island in northern Canada. Colours on map correspond to geological units in (b). **b)** Composite stratigraphic section of the Shaler Supergroup (*after* Rainbird et al., 1996, Fig. 2). **c)** Geology of NTS 87-H/05 (box on (a)) (*modified from* Rainbird et al., work in progress, 2012).

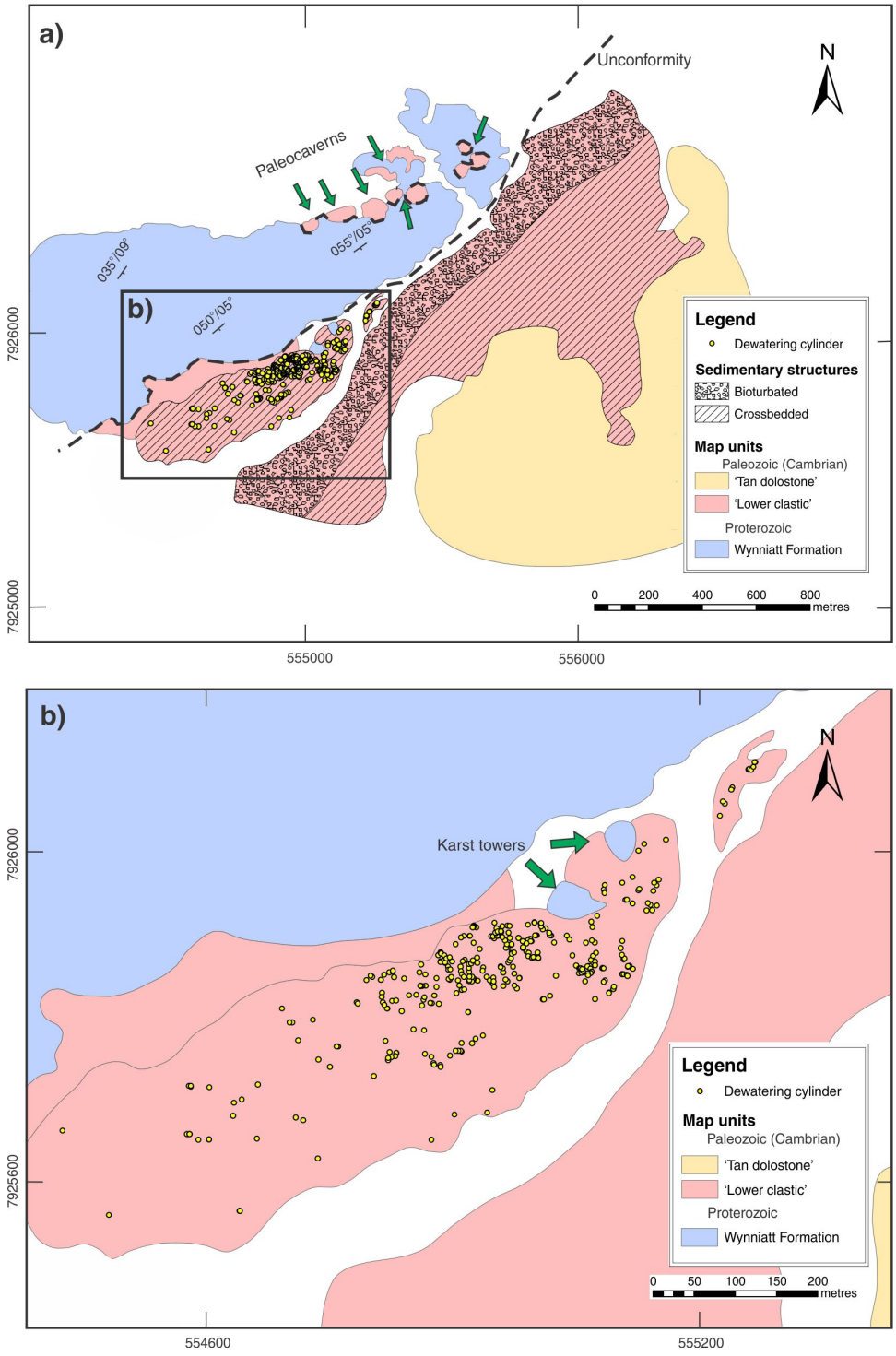

Figure 2. a) Map of the paleokarst area, showing distribution of paleocaverns and dewatering cylinders. The unpatterned pink area between Wynniatt Formation dolostone and cylinder-bearing sandstone is an area of frost-heaved sandstone rubble that could not be mapped. **b)** Detailed map of crossbedded sandstone unit showing sand-cylinder distribution.

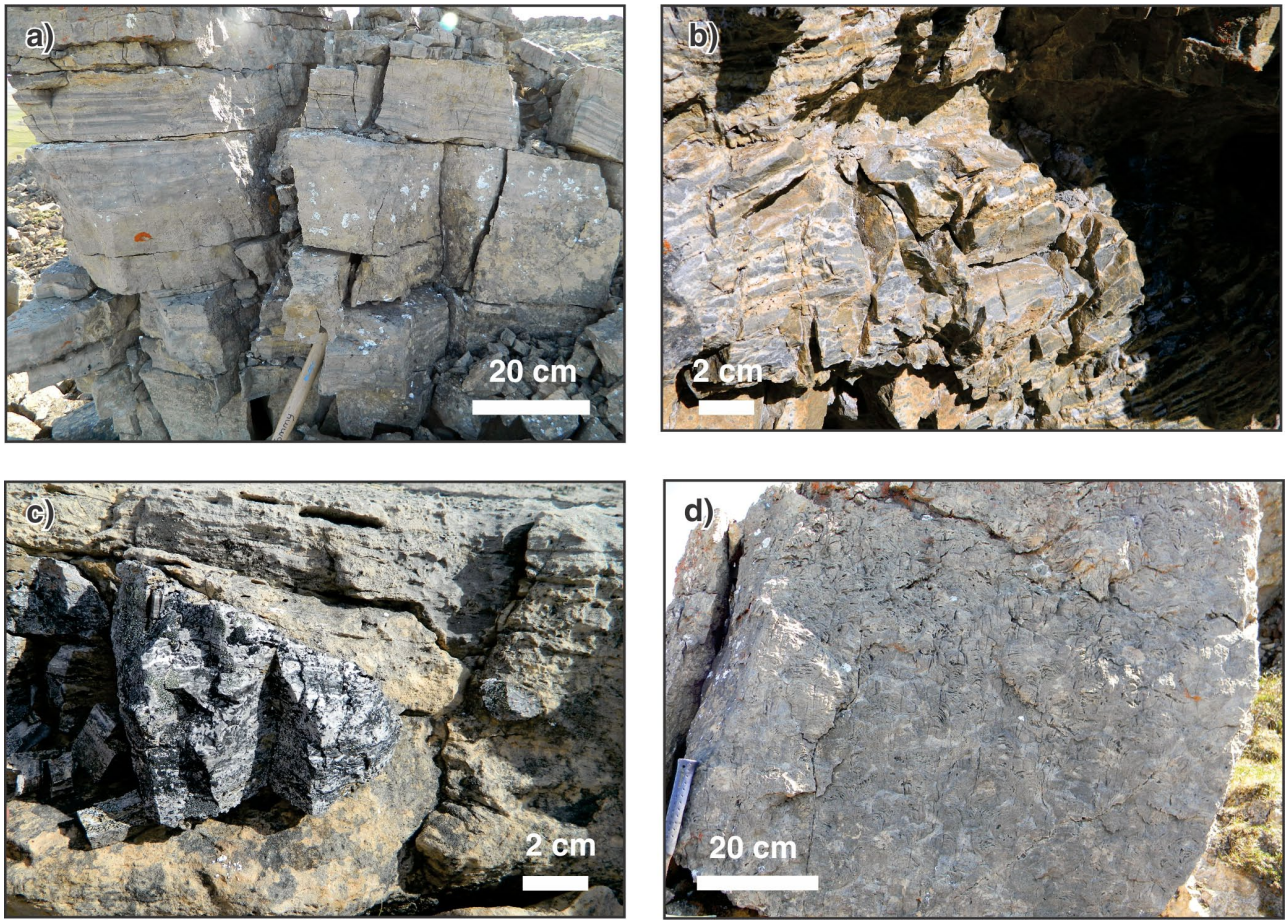

Figure 3. Typical features of the Wynniatt Formation in the study area. **a)** Pale grey dolostone with laminations and partings. 2012-169 **b)** Zebra dolomite. 2012-155 **c)** Chert nodules. 2012-167 **d)** Columnar branching stromatolites. 2012-170. All photographs by J. Mathieu.

(Fig. 3c), and columnar branching stromatolites (Fig. 3d) typify the Wynniatt Formation at this location. Hydrothermal dolomite veins and masses locally are conspicuous.

Sparry dolomite is present throughout the Wynniatt Formation regionally, but seems to be more abundant in the vicinity of the paleokarst surface. At outcrop scale, the dolomite exhibits three phases: tan-coloured, white, and brown saddle dolomite (Fig. 4a). The dolomite occupies veins that can be parallel to bedding or at various orientations to it (Fig. 3b, 4b). Local breccia masses (Fig. 4c) and small amounts of sulphide minerals (pyrite; Fig. 4d) are associated with the dolomite. It was difficult to assess in the field if the sparry dolomite masses and veins cut across the unconformity, owing to the contrasting composition of the overlying material (sandstone).

Lower Cambrian 'clastic member'

The Cambrian clastic member is divided here for simplicity into three sections at this site: basal crossbedded, bioturbated, and upper crossbedded sandstone. The basal crossbedded section is a mature, purple-red (weathered) and pale grey-purple (fresh) crossbedded sandstone, characterized by medium-sized, well sorted, rounded grains, with coarse-grained foresets (Fig. 5a). The base of this section at this site includes approximately 0.1 to 0.5 m of poorly sorted quartz-pebble conglomerate (Fig. 5b). The bioturbated interval is grey-red sandstone, made up of fine to medium-sized, well sorted, rounded grains, with vertical burrows (Fig. 5c; possibly *Skolithos*; A. Durbano, pers. comm., 2011). The upper crossbedded section is grey to grey-tan crossbedded sandstone, made up of medium-sized, well sorted, rounded grains (Fig. 5d). The upper contact with the 'tan carbonate' member is concealed by Quaternary cover at this location, but elsewhere it is sharp.

Sandstone cylinders

The basal crossbedded sandstone in the study area contains numerous large cylindrical sand structures. These cylinders have circular cross-sections with diameters of 10 cm to 14 m (Fig. 6a, b, c, d) and sharply cut across the bedding of the sandstone. The vertical cylinder walls are of unknown height (the greatest height observed was

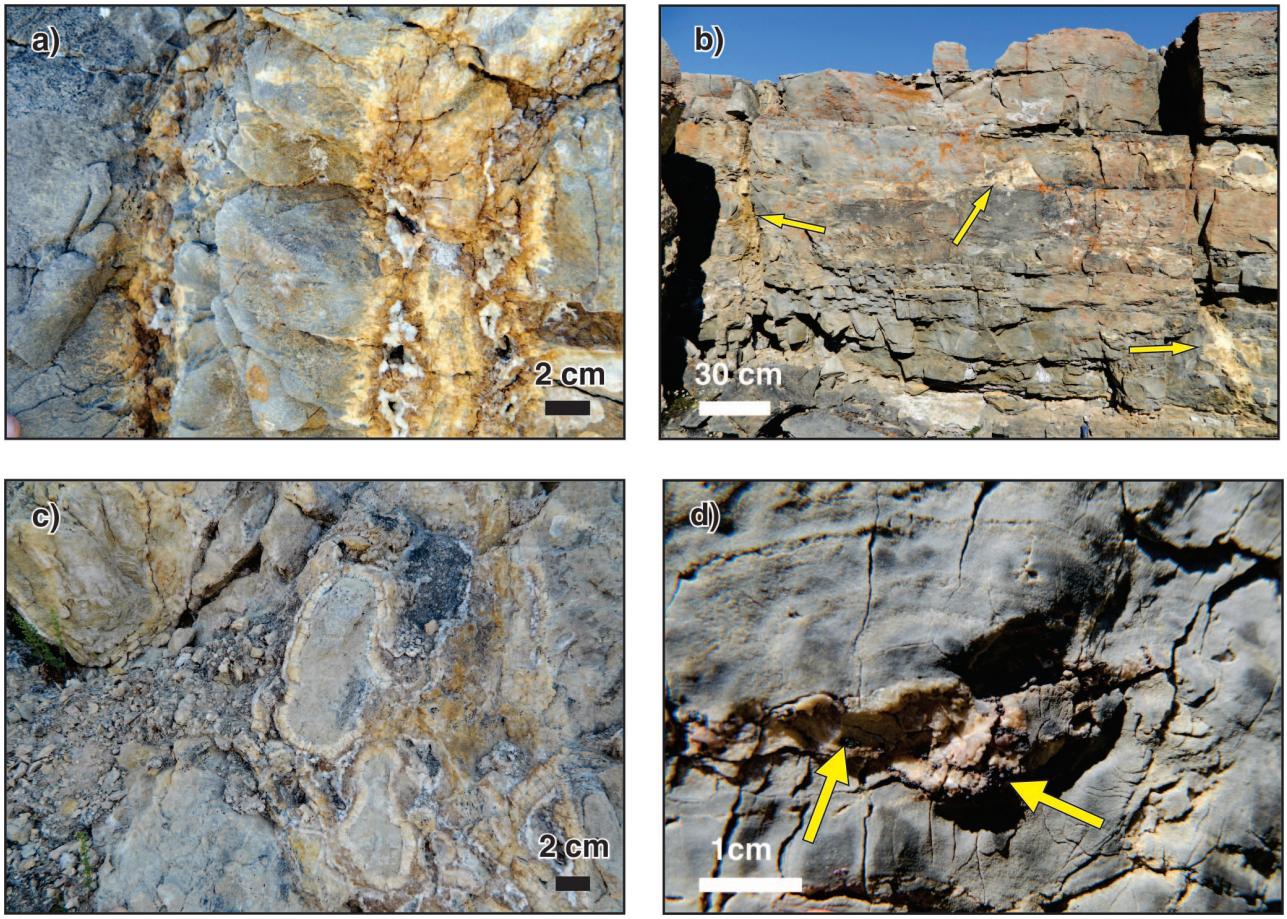

Figure 4. Hydrothermal dolomite appears to be particularly abundant in the vicinity of the unconformity. **a)** Three dolomite phases are distinguished in the field based on colour: tan, brown, and white. 2012-159 **b)** Large vertical and horizontal dolomite veins (arrows). 2012-156 **c)** Hydrothermal brecciation. 2012-154 **d)** Minor sulphide minerals (mostly pyrite?) in dolomite veins (arrows). 2012-161. All photographs by J. Mathieu.

approximately 1.5 m). The size and location of 382 of these structures was recorded (Fig. 2; Table 1). The mode and average diameter of all the cylinders are 130 cm and 60 cm, respectively, with a range between 10 cm and 16 m. The cylinders are exposed in an area of approximately 120 000 m^2 and are most abundant in the northern part (292 cylinders) of the sandstone unit, and diminish in number (but not in size) to the southwest (30 cylinders; Fig. 2). The average diameter of the cylinders from the southern exposure of the sandstone unit is 190 cm, with a mode of 100 cm (10 counts) and a range from 10 cm to 970 cm. In the northern exposure of the sandstone unit, the average diameter of the cylinders is 120 cm with modes of 40 and 60 cm (24 counts each) and a range from 10 cm to 16 m.

The core of these structures is moderately to well sorted, medium-grained sandstone, with centimetre-scale concentric banding. Many of these structures include one band of gravel- to pebble-sized clasts; a few have more than one band of coarse material. These bands of coarse material are not preferentially located within the circular cross-section; central, marginal, and intermediate positions were all documented. Cylinders locally cut across other cylinders. Rarely, a small cylinder is present inside a larger one, cross-cutting the larger structure's concentric laminae. Small (approximately 10 cm diameter), steep-sided cone structures with a relief of approximately 3 cm above the bedding plane of the sandstone are locally preserved (Fig. 6c). Cylindrical structures are absent in the bioturbated and upper crossbedded sections.

Unconformity

The base of the Cambrian sandstone is represented by an irregular unconformity surface in sharp contact with underlying strata of the Wynniatt Formation. Paleokarst features such as grykes, caverns, pans, and towers are preserved locally within the Wynniatt Formation. Grykes, solution-widened joints in carbonate rocks created via interaction with meteoric water (James and Choquette, 1990), locally penetrate the upper surface of the Wynniatt Formation and can be parallel or perpendicular to dolostone bedding (Fig. 7a), creating a complex network. These networks are

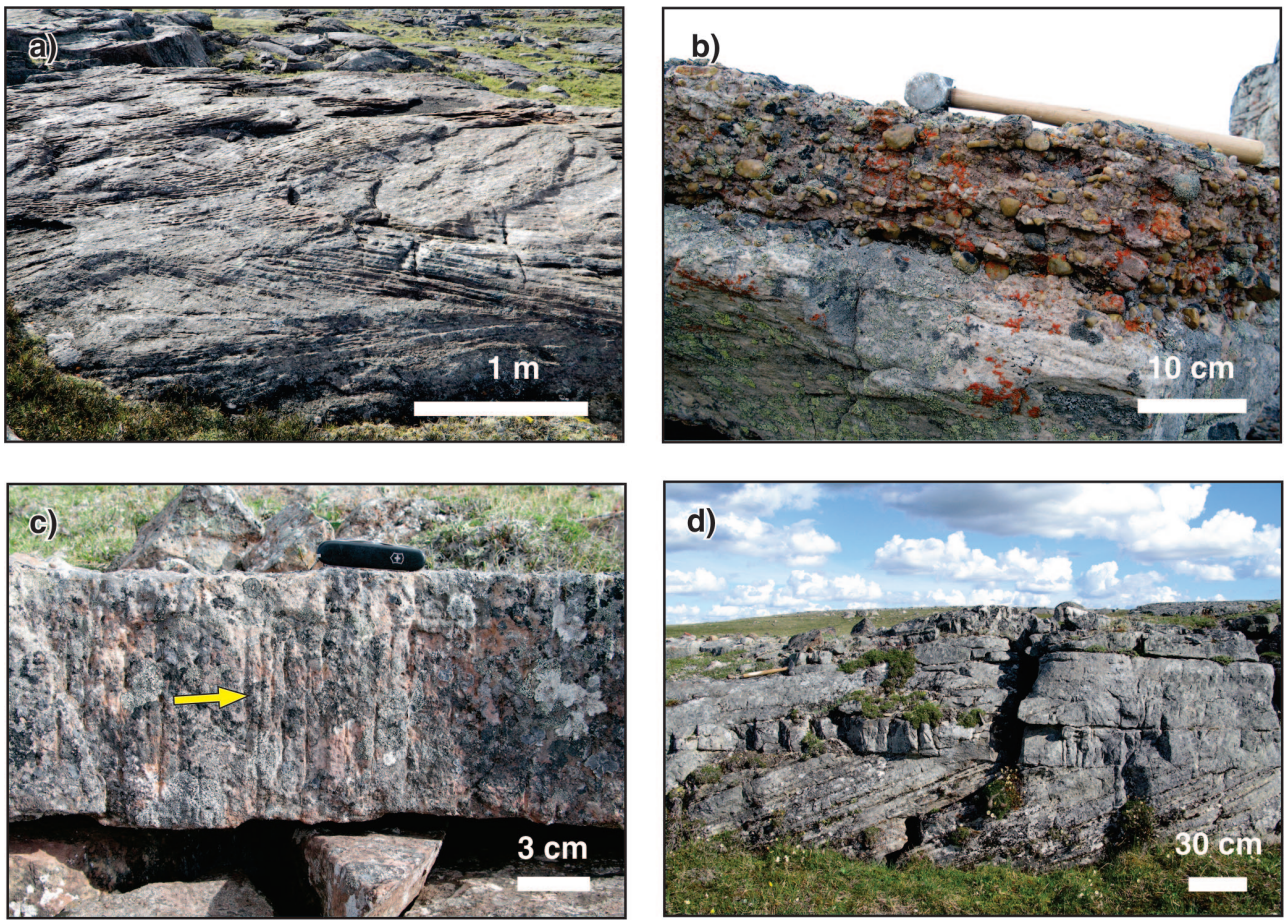

Figure 5. Cambrian 'lower clastic member'. **a)** Basal, planar crossbedded quartz arenite. 2012-160 **b)** Conglomerate bed at the base of the crossbedded quartz arenite. 2012-168 **c)** Bioturbated section with vertical burrows (*Skolithos*). 2012-151 **d)** Upper crossbedded section above the bioturbated section. 2012-152. All photographs by A. Durbano.

filled with medium-grained hematitic sandstone. Individual grykes are from one centimetre to several decimetres wide and one metre to decimetres deep. Similar gryke networks in dolostone have also been documented below the base of the Cambrian sandstone elsewhere on Victoria Island.

Sandstone-filled paleocaverns are present along the edge of a northwest-striking ridge of Wynniatt Formation over a distance of approximately 1 km (Fig. 2, 7b). The paleocaverns are roughly circular in cross-section, with apparent 'diameters' of approximately 30 to 100 m (Fig. 7c). Surfaces within these paleocaverns have concave dish-shaped depressions, which may be preserved dissolution pans (James and Choquette, 1990; Fig. 7d). The caverns' paleofloors are not exposed; their paleoroofs are approximately 10 to 15 m below the main surface of the unconformity. Recent erosion has cut obliquely across the sand-filled caverns, providing exposures of their walls and ceilings. The walls display overhanging remnants of cave walls (Fig. 7b). The fill of these features is dominated by sandstone and pebbly sandstone that is identical to that in the basal Cambrian sandstone. Blocks of Wynniatt Formation and sediment of any composition other than sandstone are lacking.

There are two isolated, narrow, relatively high-relief (4 to 5 m above the stratigraphic contact) units of Wynniatt Formation upper carbonate that protrude above the nominal stratigraphic level of the unconformity into the Cambrian sandstone (Fig. 2); these could possibly be remnants of paleokarst towers (Sweeting, 1972).

INTERPRETATION

Cylindrical structures

These structures are interpreted as feeder conduits for sand volcanoes. The cylinders formed after the sand was deposited over the karst surface but before the sand lithified. Pulses of water from submarine springs fluidized sediment, moving it upward and through the unconsolidated sand. This truncated bedding and created sand volcanoes on the seafloor. The inconsistent strength of the water movement caused concentric rings of coarse material to rise in the feeder-zone pipes of the volcanoes. The coarser bands represent pulses of higher water flow and the finer bands, pulses of lower water flow. Because the water appears to have come

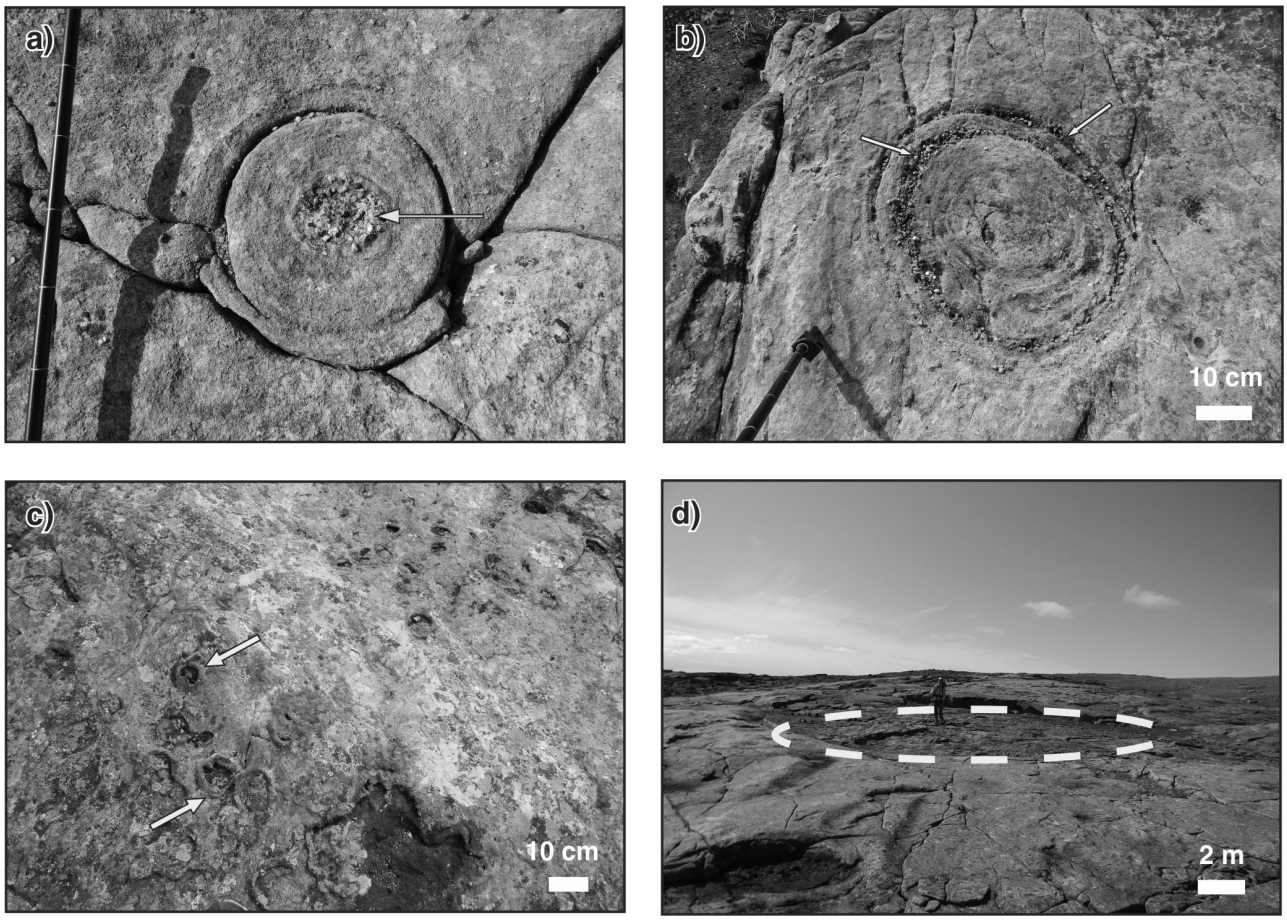

Figure 6. Cylinders in the Cambrian sandstone. **a)** Cross-section of cylindrical column with coarse gravel at its core (arrow). Pole is marked in 10 cm increments. 2012-162 **b)** Cross-section of column with two concentric zones of coarse gravel (arrows). 2012-166 **c)** Sand volcanoes on a bedding plane. 2012-158 **d)** Exposure of column approximately 15 m in diameter (person for scale). 2012-153. All photographs by J. Mathieu.

from the underlying Wynniatt Formation karst reservoir, gravel-grade material from the base of the sandstone was carried up the pipes when fluid flow rates were great enough to transport it.

Numerous studies have documented cylindrical structures in a variety of settings. Cylinders have been documented from the Cambrian Potsdam Formation (Hawley and Hart, 1934; Sanford and Arnott, 2010), Permian Talchir Formation (van Loon and Maulik, 2011), younger rocks from Colorado (Gabelman, 1955) and Nebraska (Guhman and Pederson, 1992), and in modern sediment along the Mississippi River (Li et al., 1996) and in Tuchodi Lake, British Columbia (Long and Donaldson, 2005). The means by which these cylinders developed is controversial, particularly with respect to the mechanism of fluidization. Experimental studies of fluidization have attempted to re-create cylindrical structures in sediment (Hawley and Hart, 1934; Nichols et al., 1994; Owen, 1996; Buck and Goldring, 2003; Kadau et al., 2009; Ross et al., 2011) with variable success.

Sand volcanoes in the Talchir Formation, India (van Loon and Maulik, 2011) resemble the Minto Inlet structures, but occupy a smaller geographic area (50 m^2 vs. 120 000 m^2). Sediment liquefaction in the Indian example was attributed to a seismic event. Because a seismic event would normally have caused soft-sediment deformation, it was argued that the area was far enough away from the epicentre of the shock to liquefy the sand, but not create seismites. Because a sand-volcano field like the one described by van Loon and Maulik (2011) was produced at the Victoria Island location, and no other soft-sediment deformation is evident, a similar trigger could be invoked for the Minto Inlet structures. However, the pulsing nature of the fluidized sediment, suggested by the concentric rings of coarser material, together with the local crosscutting relationships between pipes, cannot be explained by a single, instantaneous fluidization caused by a single seismic event. It could be argued that multiple seismic events could account for the pulsing flow or the crosscutting relationships between cylinders. However, the spatial distribution of the cylinders — that is, decreasing from north to south — must also be taken into consideration. If multiple seismic events occurred as a result of movements along the

Table 1. Diameter and UTM co-ordinates of dewatering cylinders in Cambrian sandstone near Minto Inlet.

Diameter (cm)	Easting	Northing
100	554396.23	7925567.22
160	554340.095	7925669.651
150	554494.86	7925724.06
480	554577.13	7925725.97
340	554518.13	7925722.42
120	554495.863	7925723.058
100	554493.383	7925724.032
95	554495.87	7925724.062
120	554557.39	7925707.61
560	554547.89	7925703.47
260	554547.1	7925687.83
340	554517.72	7925659.19
160	554518	7925659.19
120	554505.04	7925658.86
120	554490.88	7925665.76
200	554576.08	7925660.11
90	554493.88	7925665.76
90	554494	7925665.76
450	554554.65	7925572.54
90	554555	7925572.54
260	554649.84	7925635.95
90	554632	7925682.36
220	554664.49	7925747.16
300	554674.59	7925771.96
40	554672.59	7925771.96
160	554650.47	7925756.106
100	554626.04	7925779.28
140	554623.04	7925685.992
30	554618.6	7925801.4
150	554643.95	7925804.47
80	554615.6	7925801.4
60	554606.27	7925818.01
200	554855.52	7925691.59
150	554787.72	7925658.8
500	554815.92	7925689.28
970	554861.46	7925718.89
320	554850.16	7925785.18
190	554841.36	7925781.6
270	554836.89	7925775.91
110	554824.34	7925765.92
300	554823.34	7925766.92
130	554820.34	7925766.92
450	554817.34	7925766.92
220	554810.47	7925761.1
100	554798.39	7925749.27
90	554798.61	7925747.41
35	554790.27	7925751.66
50	554791.02	7925749.82
200	554717.64	7925736.05
120	554780.02	7925762.93
100	554787.88	7925759.23
100	554824.36	7925776.52
35	554832.49	7925813.55
25	554832.09	7925813.55
490	554778.87	7925791.72
200	554745.44	7925763.91
400	554745.04	7925763.91
270	554736.93	7925765.18
210	554743.7	7925760.33
55	554739.41	7925758.92
200	554735.22	7925755.65
120	554735.28	7925758.07
370	554732.02	7925778.81
390	554766.1	7925792.89
25	554796.72	7925823.79

Table 1. (Continued)

Diameter (cm)	Easting	Northing
190	554787.99	7925824.69
100	554786.44	7925825.02
130	554778.16	7925828.9
240	554776.26	7925821.97
70	554751.73	7925815.02
100	554696.93	7925825.53
25	554698.33	7925824.07
20	554734.05	7925817.92
30	554733.65	7925817.92
70	554728.58	7925825.59
100	554730.85	7925822.49
60	554727.57	7925837.28
40	554727.47	7925832.07
130	554740.1	7925827.18
60	554760.6	7925834.21
130	554769.48	7925834.81
130	554779.16	7925831.71
200	554791.19	7925833.88
170	554793.92	7925854.78
130	554794.01	7925844.36
160	554780.7	7925845.7
90	554776.91	7925845.42
60	554774.84	7925845.18
95	554774.44	7925845.58
55	554774.2	7925845.58
390	554744.7	7925828.04
50	554709.05	7925852.43
130	554716.11	7925856.7
170	554713.94	7925858.13
35	554726.4	7925853.05
35	554726.3	7925853.05
75	554730.28	7925858.92
130	554736.42	7925862.05
60	554742.2	7925856.25
40	554741.09	7925862.73
70	554741.09	7925864.23
220	554754.69	7925854.52
55	554775.12	7925871.59
55	554773.17	7925862.06
135	554780.4	7925859.45
60	554796.16	7925882.91
20	554798.86	7925886.33
35	554798.86	7925885.73
40	554799.36	7925885.13
15	554799.46	7925885.13
240	554803.41	7925882.35
30	554803.41	7925882.45
40	554798.79	7925875.36
60	554798.79	7925874.86
30	554798.79	7925874.56
120	554803.09	7925876.4
70	554804.35	7925873.45
60	554804.35	7925874.15
130	554807.76	7925878.93
250	554806	7925878.93
50	554810.16	7925880.3
70	554812.61	7925874.96
70	554807.96	7925868.9
220	554808.23	7925865.18
70	554810.77	7925865.43
130	554823.13	7925869.1
160	554823.69	7925863.35
60	554824.55	7925859.83
160	554827.12	7925856.55
60	554810.03	7925852.77

Table 1. (Continued)

Diameter (cm)	Easting	Northing
40	554808.52	7925854.03
60	554811.84	7925856.16
120	554811.84	7925856.26
200	554819.88	7925852.28
10	554818.32	7925836.8
70	554824.27	7925840.49
50	554824.63	7925840.5
120	554827.4	7925841.13
30	554821.46	7925846
100	554843.83	7925851.96
90	554838.48	7925852.57
160	554839.21	7925854.26
50	554837.51	7925853.47
40	554836.62	7925851.22
140	554833.12	7925851.5
50	554833.92	7925852.45
50	554837.07	7925856.81
110	554833.92	7925857.1
320	554833.54	7925862.85
30	554833.19	7925867.12
80	554833.13	7925871.96
80	554836.13	7925872.78
300	554828.19	7925877.22
40	554825.58	7925875.3
260	554817.34	7925896.28
150	554838.06	7925876.17
50	554838.06	7925876.37
140	554843.18	7925879.84
240	554843.58	7925873.52
420	554850.66	7925867.75
40	554849.98	7925864.2
60	554854.97	7925856.71
60	554854.87	7925856.71
100	554858.35	7925852.14
70	554862.88	7925855.61
190	554862.42	7925848.16
150	554863.02	7925847.99
30	554863.41	7925851.34
50	554863.94	7925844.29
560	554875.06	7925845.32
410	554880.19	7925851.03
160	554879.99	7925851.23
35	554877.64	7925853.38
80	554874.57	7925862.23
70	554874.87	7925862.23
130	554874.21	7925866.87
180	554871.66	7925869.22
60	554871.66	7925868.12
400	554839.1	7925897.96
40	554834.03	7925906.19
30	554834.63	7925906.19
120	554826.92	7925906.2
330	554823.77	7925904.45
100	554842.54	7925916.64
100	554839.52	7925918.79
110	554839	7925918.41
40	554839	7925917.51
30	554838.4	7925917.51
40	554838.4	7925917.11
20	554837.9	7925917.11
30	554837.5	7925916.71
50	554846.35	7925890.33
200	554891.19	7925842.57
80	554888.73	7925846.04
140	554894.78	7925855.31

Table 1. (Continued)

Diameter (cm)	Easting	Northing
20	554894.38	7925854.91
90	554888.31	7925860.35
50	554888.71	7925860.35
210	554886.79	7925868.86
90	554881.21	7925873.56
210	554882.39	7925876.37
90	554884.21	7925879.21
150	554885.13	7925887.23
60	554885	7925885.37
40	554885	7925884.77
70	554888.06	7925886.19
80	554880.2	7925892.5
50	554878.26	7925891.89
50	554883.73	7925895.75
60	554883.93	7925895.75
30	554884.93	7925895.75
20	554884.93	7925896.15
60	554879.21	7925896.19
150	554876.79	7925900.59
110	554874.01	7925904.8
110	554868.41	7925906.14
90	554863.85	7925903.61
50	554860.12	7925905.75
50	554862.61	7925905.81
100	554867.28	7925906.3
130	554866.01	7925909.43
360	554865.4	7925910.16
400	554864.26	7925922.4
310	554866.63	7925915.4
90	554868.03	7925911.53
310	554872.72	7925911.46
50	554872.22	7925911.96
50	554873.91	7925918
230	554880.05	7925918.9
90	554882.37	7925918.59
65	554882.93	7925903.72
30	554881.28	7925910.19
330	554893.42	7925903.81
130	554893.42	7925903.71
60	554898.79	7925899.85
60	554898.49	7925899.85
70	554898.65	7925891.48
120	554898.65	7925891.78
70	554898.65	7925892.48
90	554902.85	7925887.13
40	554905.62	7925885.71
180	554905.31	7925881.42
220	554909.68	7925879.68
70	554910	7925879.68
230	554909.68	7925879.58
160	554916.46	7925881.15
100	554916.69	7925885.99
60	554912.81	7925880.13
20	554911.81	7925880.13
40	554911.81	7925880.43
20	554911.61	7925880.43
100	554917.7	7925878.95
90	554917.7	7925879.45
320	554923	7925829.44
160	554924.1	7925829.44
320	554931.6	7925833.56
500	554938.8	7925858.11
110	554936.58	7925898.4
70	554933.41	7925906.5
170	554931.39	7925906.82

Table 1. (Continued)

Diameter (cm)	Easting	Northing
350	554930.49	7925909.78
70	554926.55	7925915.25
110	554922.85	7925914.04
280	554921.03	7925917.9
110	554920.46	7925921.61
90	554921.18	7925921.44
95	554921.18	7925922
60	554912.96	7925922.9
60	554912.96	7925922.4
55	554912.96	7925922.2
90	554904.86	7925919.91
45	554907.43	7925902.86
180	554904.87	7925901.12
140	554909.05	7925899.74
10	554908.05	7925899.74
350	554903.31	7925897.18
350	554915.44	7925906.97
90	554914.44	7925906.97
110	554913.54	7925906.97
80	554952.14	7925906.42
160	554955.34	7925901.86
230	554959.04	7925882.61
250	554963.38	7925870.45
35	554967.03	7925866.82
100	554968.53	7925866.82
30	554968.73	7925866.82
380	554966.95	7925860.68
80	554969.76	7925861.69
25	554969.76	7925861.59
25	554970.01	7925861.59
30	554971.8	7925863.39
240	554970.61	7925865.8
240	554978.25	7925868.41
70	554978.25	7925869.41
50	554978.35	7925869.51
30	554978.75	7925868.51
40	554980.15	7925869.51
100	554976.98	7925869.12
110	554980.67	7925866.43
130	554982	7925862.93
20	554982.3	7925862.63
40	554982.6	7925862.63
50	554981.1	7925861.13
30	554981.3	7925861.13
90	554977.21	7925860.39
60	554977.11	7925860.31
110	554977.41	7925860.39
160	554977.31	7925860.59
300	554977.73	7925858.36
320	554974.42	7925851.02
590	554986.11	7925829.75
370	555003.46	7925837.44
160	555008.38	7925841.85
100	555003.18	7925836.69
320	555009.32	7925844.66
80	554998.57	7925852.2
340	554996.72	7925850.66
360	554995.18	7925866.8
110	554995.58	7925867.2
40	554995.58	7925867.3
60	554981.58	7925877.05
230	554983.83	7925881.94
80	554975.17	7925898.09
140	554981.99	7925923.55
40	554996.93	7925962.61

Table 1. (Continued)

Diameter (cm)	Easting	Northing
160	554998.16	7925968.04
210	554998.02	7925959.3
100	554998.02	7925958.6
30	554989.09	7925930.8
140	554983.28	7925917.08
80	554985.89	7925898.36
150	554982.45	7925900.88
200	554987.64	7925885.58
40	554986.25	7925875.13
120	554986.31	7925870.66
220	554996.95	7925867.03
30	555019.41	7925859.98
140	555019.49	7925859.43
50	555021.26	7925859.66
60	555024.89	7925859.01
170	555025.64	7925857.72
140	555032.06	7925866.26
170	555028.41	7925869.88
40	555026.24	7925868.71
140	555026.24	7925869.71
100	555021.49	7925878.45
45	555021.2	7925878.45
90	555020.98	7925877.69
40	555021.98	7925878.69
90	555019	7925883.22
160	555017.31	7925891.36
65	555019.52	7925899.97
90	555023.28	7925949.9
40	555024.78	7925950.4
120	555031.85	7925945.84
180	555019.31	7925970.63
40	555031.81	7925977.45
270	555038.74	7925961.64
65	555039.83	7925963.16
260	555053.59	7925944.17
100	555050.63	7925946.14
110	555048.78	7925937.35
90	555055.48	7925937.52
125	555061.26	7925943.06
180	555057.13	7925961
70	555060.99	7925967.6
150	555057.88	7925970.87
280	555063.36	7925974.54
180	555038.93	7926009.81
140	555046.13	7926017.8
1600	555072.42	7926023.13
220	555138.06	7926051.96
40	555143.65	7926067.17
180	555141.52	7926069.53
60	555153.12	7926086.38
185	555151.58	7926083.73
110	555172.52	7926108.26
90	555173.52	7926109.26
60	555175.85	7926108.16
130	555178.72	7926111.58
40	555180.53	7926117.39
30	555180	7926117.39

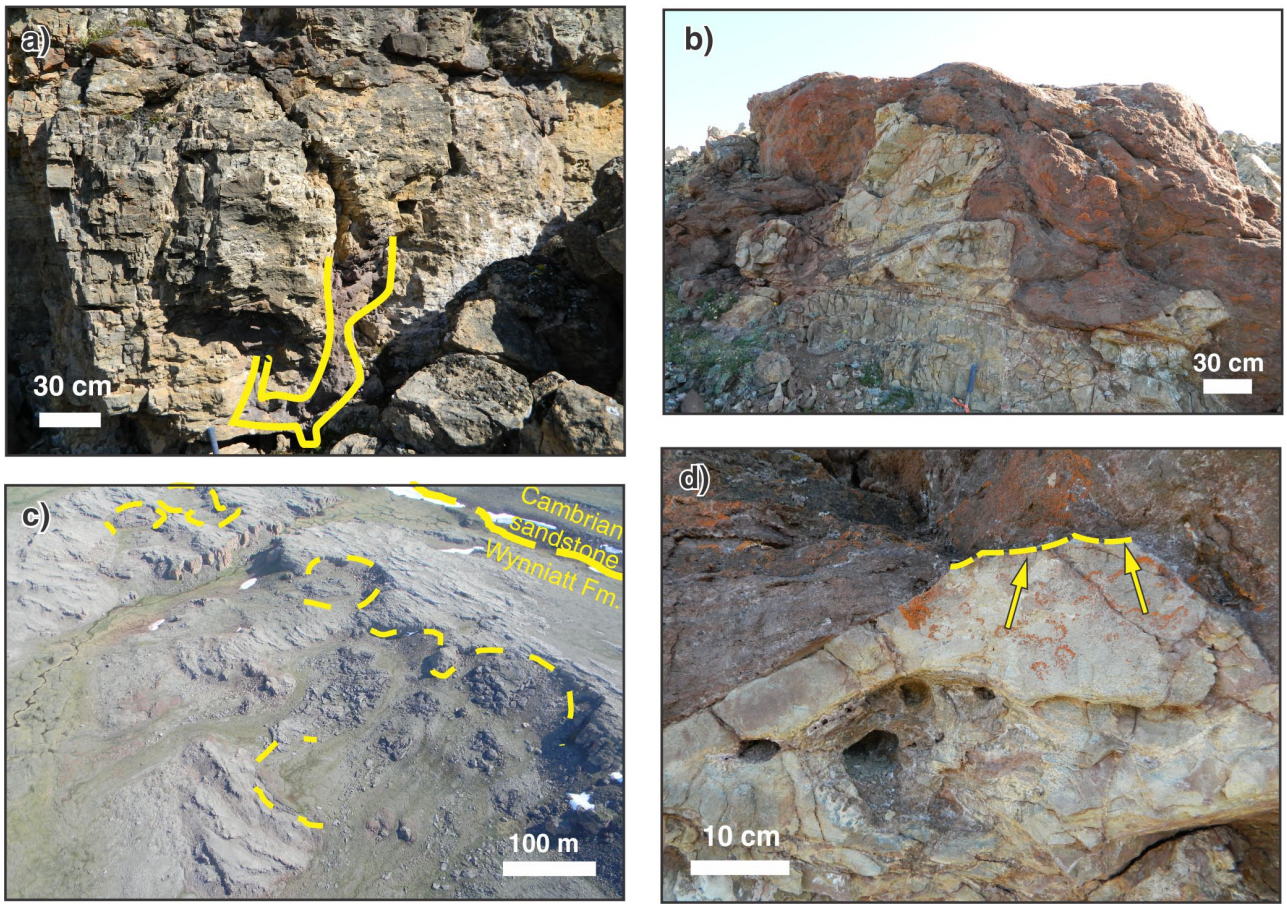

Figure 7. Karstic features below the Proterozoic–Cambrian unconformity. **a)** Vertical cross-section of a gryke that branches into vertical and horizontal orientations. 2012-164 **b)** Sharp, irregular paleocavern base and wall. 2012-165 **c)** Aerial view of the karst area showing red-sandstone–filled paleocaverns in Wynniatt Formation, well below the projected stratigraphic contact of Wynniatt Formation and red sandstone of the basal Cambrian unit. 2012-157 **d)** Dissolutional scalloping on paleohorizontal surface within a paleocavern (arrows). 2012-163. All photographs by J. Mathieu.

nearby faults (Fig. 1c), the expected distribution should be either even or showing a decrease in abundance from south to north (since the nearest fault is just to the south of the study area).

Clustered cylindrical dewatering structures in a Pleistocene calcarenite that overlies karsted carbonate rock in Salento, Italy were documented by Massari et al. (2001). These cylinders were interpreted to have formed when water upwelled from an underlying karst reservoir. Because the cylinders were clustered, had circular cross-sections, and were composed of sand capable of dispersing excess pore pressure, Massari et al. (2001) rejected a seismic model. The lack of concentric downfaulting or association with soft-sediment deformation led Massari et al. (2001) to reject a model involving collapse of caves to infill the underlying karst. The Minto Inlet cylinders, like the Italian structures, are clustered, are circular in cross-section, lack concentric downfaulting patterns or soft-sediment deformation (with one exception), and formed in a pressure-dispersing medium. Because of the similarities, the arguments against seismic and/or cave-collapse origins could similarly be made here. There is one large cylinder among the Victoria Island cylinders that displays an apparent dipping of beds in toward the centre of the structure; concentric banding was not observed in this structure due to vegetative cover. This single occurrence may have been formed through collapse of an underlying karst feature and would then be considered an isolated event.

Li et al. (1996) discussed conical extrusive structures with cylindrical structures under them in sands alongside the levees of the Mississippi River. They interpreted the structures as sand boils formed by the flooding of the Mississippi River in 1993. They determined that the large hydraulic head caused by the high artificial levee caused fluid flow under the levee to produce sand boils on the floodplain. The boils were most densely distributed close to the levee, and diminished in both size and number away from the levee (maximum distance from levee was ~100 m). The concentration of the Minto Inlet volcanoes is highest in the northern part of the mapped area and decreases to the southwest, resembling the

distribution noted by Li et al. (1996). Submarine springs appear to exhibit the same spatial distribution as the sand boils of a flooding river: they are most abundant closest to the shore (Fritz and Bahun, 1997; Bayari and Kurttas, 2002; Bayari et al., 2011). In the study of Fritz and Bahun (1997), groundwater was transported through a paleokarst network to submarine springs.

Repeated upward movement of sediment in the Minto Inlet cylinders is indicated by the presence of gravel in the concentric bands of the cylinders (probably derived from a base of clastic unit; Fig. 6a, b), along with the single small group of sand volcanoes preserved on a bedding plane (Fig. 6c). This provides evidence against models which involve collapse of overlying sands into voids as the mechanism to create these cylinders. The nonlinear distribution of the cylinders, their circular cross-sections, the good to moderate sorting of the sand, and the southwestward decrease in abundance (Fig. 2b) are some of the criteria Li et al. (1996) used in arguing against seismically induced cylinder formation. Although there are faults present around the study area that are assumed to have been active in the Cambrian (Fig. 1c) and could be responsible for some isolated instances, the arguments presented here favour a different mechanism of formation for the whole area. The Minto Inlet cylinders more closely resemble the sand volcanoes produced by Mississippi River flooding (Li et al., 1996) and the submarine springs of Fritz and Bahun (1997); they are interpreted as the result of meteoric groundwater flow, concentrated within karst features in the Wynniatt Formation. The flow was driven by a hydraulic head, produced by accumulation of rainwater beneath the nearby carbonate land surface (a freshwater lens) at the time when basal Cambrian sand had just begun to accumulate over the unconformity. The water emerged onto the shallow seafloor as point sources of fresh water (subaqueous springs). The fresh water rose through the sandy sediment and overlying salt water in a temporally variable manner (pulsing), driven by pressure variations in the hydraulic head. The rising freshwater plume fluidized the sandy sediment, caused upward migration of sand to produce cylindrical channels with crude concentric lamination, and forced pebbles to rise from their position near the basal contact. Conical sand volcanoes would have been expected to develop on the upper surface of the sand (they are rare here due to erosion).

Hydrothermal dolomite

Field observations of the apparent truncation of hydrothermal dolomite veins by karst features, and of hydrothermal dolomite occupying void space around sand fill, provide ambiguous evidence regarding the temporal relationship between the dolomitizing hydrothermal fluid and paleokarst development: there appears to be evidence for migration of hydrothermal fluid both before and after development of the unconformity. The timing and origin of the dolomite phases are consequently unknown, and will be addressed by further study.

Karst evolution

During the early Neoproterozoic, when the Shaler Supergroup was deposited, and in the early Cambrian, Laurentia was at a low latitude (~10°; Park, 1994; Irving et al., 2004). There is evidence for both arid climates (Kilian Formation sabkha evaporites; Young, 1981) and humid climates (Kuujjua Formation fluvial sandstone; Rainbird, 1992a, 1993) during deposition of the uppermost Shaler Supergroup (above the Wynniatt Formation). After eruption of the Natkusiak Formation lavas on top of the Kuujjua and Kilian formations at ca.720 Ma (Heaman et al., 1992), there was folding and uplift followed by erosional removal of several kilometres of Neoproterozoic strata, which exposed the upper Wynniatt Formation in the study area. Rainwater and groundwater gradually dissolved the carbonate bedrock of the Wynniatt Formation to form karst features such as grykes, towers, and caverns (Fig. 8a). Karstification occurred either late in the Neoproterozoic or, more probably, early in the Cambrian, just prior to transgression and deposition of the sandstone, accounting for preservation of the karst features. Preservation of the cavern system at a stratigraphic position several tens of metres below the unconformity strongly suggests its development at a water table that was associated with a freshwater lens, shortly before deposition of the sandstone. Relative sea level rose, submerging the karstified surface of the Wynniatt Formation and filling the caverns and grykes with quartzose sand, and deposited sandstone layers above the unconformity. Fresh water was collected over exposed land immediately north of the mapped area and moved through the Wynniatt Formation using the joints and karst features as conduits to feed the submarine springs. The hydraulic head in the karst network was sufficient to fluidize the sediment in and above the karst and mobilize it to propagate upward toward the seafloor, where it produced submarine springs and sand volcanoes (Fig. 8b). The presence of bioturbation in fine- to medium-grained sandstone that overlies the cylinder-bearing interval suggests a sea-level rise, placing this location in an open marine, subtidal setting. The extended distance from the coastline produced by sea-level rise subdued the topographically driven hydraulic head, and springs in the area became inactive, as low flows would have diffused through unconsolidated sands.

CONCLUSIONS

A deeply karstified unconformity separates the Neoproterozoic Wynniatt Formation (dolostone) from lower Cambrian sandstone. Several common karst features are well developed: dissolution pans on the surface of the Wynniatt Formation, gryke networks, towers, and paleocaverns. The contact with the overlying Cambrian marine sandstone is

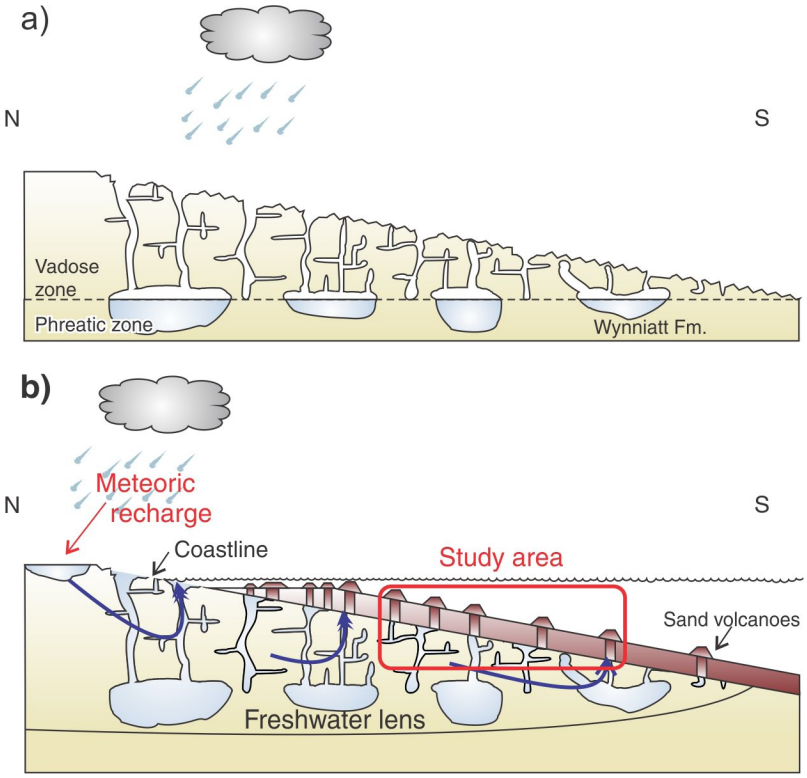

Figure 8. Interpretation of karsting and sand-cylinder formation. **a)** Late Neoproterozoic or early Cambrian erosion of overlying formations exposed the Wynniatt Formation to meteoric dissolution, creating a karst environment. **b)** Cambrian sand deposited over the karst surface was reworked locally by submarine springs formed due to the hydraulic head to the north (left) of the coastline forcing water through the karst features as conduits.

sharp and well exposed in some areas. The Cambrian sandstone unit contains cylindrical structures, decimetres to metres in diameter, which crosscut bedding perpendicularly. The cylinders are interpreted as the pipes that developed below sand volcanoes. The cylinders formed where groundwater flowing through karstic permeability pathways in the dolostone passed through unconsolidated sand and emerged onto the shallow seafloor, creating submarine springs and sand volcanoes.

Veins of hydrothermal dolomite are spatially associated with the paleokarst. The temporal relationship between the unconformity and hydrothermal fluid migration is ambiguous, and further research will be conducted to answer this question.

ACKNOWLEDGMENTS

The Geological Survey of Canada GEM Victoria Island project supported the field research. Andrew Durbano provided assistance in the field and helpful discussion as well as sharing his photos. Danielle Thomson, Dr. Darrel Long, and Dr. Keith Dewing provided valuable instruction and advice.

REFERENCES

Bayari, C.S. and Kurttas, T., 2002. Coastal and submarine karstic discharges in the Gökova Bay, SW Turkey; Quarterly Journal of Engineering Geology and Hydrogeology, v. 35, p. 381–390. doi:10.1144/1470-9236/01034

Bayari, C.S., Ozyurt, N.N., Oztan, M., Bastanlar, Y., Varinlioglu, G., Koyuneu, H., Ulkenli, H., and Hamarat, S., 2011. Submarine and coastal karstic groundwater discharges along the southwestern Mediterranean coast of Turkey; Hydrogeology Journal, v. 19, p. 399–414. doi:10.1007/s10040-010-0677-y

Buck, S.G. and Goldring, R., 2003. Conical sedimentary structures, trace fossils or not? Observations, experiments, and review; Journal of Sedimentary Research, v. 73, no. 3, p. 338–353. doi:10.1306/091602730338

Fritz, F. and Bahun, S., 1997. The morphogenesis of submarine springs in the Bay of Kastela, Croatia; Geologia Croatica, v. 50, no. 1, p. 105–110.

Gabelman, J.W., 1955. Cylindrical structures in Permian(?) siltstone, Eagle County, Colorado; The Journal of Geology, v. 63, no. 3, p. 214–227. doi:10.1086/626251

Guhman, A.I. and Pederson, D.T., 1992. Boiling sand springs, Dismal River, Nebraska: agents for formation of vertical cylindrical structures and geomorphic change; Geology, v.20, p. 8–10. doi:10.1130/0091-7613(1992)020<0008:BSSDRN>2.3.CO;2

Hawley, J.E. and Hart, R.C., 1934. Cylindrical structures in sandstones; Geological Society of America Bulletin, v. 45, p. 1017–1034.

Heaman, L.M., LeCheminant, A.N., and Rainbird, R.H., 1992. Nature and timing of Franklin igneous events, Canada; implications for a late Proterozoic mantle plume and the break-up of Laurentia; Earth and Planetary Science Letters, v. 109, no. 1–2, p. 117–131. doi:10.1016/0012-821X(92)90078-A

Irving, E., Baker, J., Hamilton, M., and Wynne, P.J., 2004. Early Proterozoic geomagnetic field in western Laurentia: implications for paleolatitudes, local rotations and stratigraphy; Precambrian Research, v. 129, p. 251–270. doi:10.1016/j.precamres.2003.10.002

James, N.P. and Choquette, P.W., 1990. Limestones – the meteoric diagenetic environment; *in* Geoscience Canada Reprint Series 4, Diagenesis, (ed.) I.A. McIlreath and D.W. Morrow, p. 35–74.

Jones, D.S., Maloof, A.C., Hurtgen, M.T., Rainbird, R.H., and Schrag, D.P., 2010. Regional and global chemostratigraphic correlation of the early Neoproterozoic Shaler Supergroup, Victoria Island, Northwestern Canada; Precambrian Research, v. 181, p. 43–63. doi:10.1016/j.precamres.2010.05.012

Kadau, D., Herrmann, H.J., Andrade, J.S., Araujo, A.D., Bezerra, L.J.C., and Mala, L.P., 2009. Living quicksand; Granular Matter, v. 11, p. 67–71. doi:10.1007/s10035-008-0117-z

Li, Y., Craven, J., Schweig, E.S., and Obermeier, S.F., 1996. Sand boils induced by the 1993 Mississippi River flood: Could they one day be misinterpreted as earthquake-induced liquefaction?; Geology, v. 24, no. 2, p. 171–174. doi:10.1130/0091-7613(1996)024<0171:SBIBTM>2.3.CO;2

Long, D.G.F. and Donaldson, J.A., 2005. Modern and ancient clastic sedimentary environments: a collection of field photographs; Geological Association of Canada, CSRG CD-1.

Long, D.G.F., Rainbird, R.H., Turner, E.C., and MacNaughton, R.B., 2008. Early Neoproterozoic strata (Sequence B) of mainland northern Canada and Victoria and Banks islands: a contribution to the Geological Atlas of the Northern Canadian Mainland Sedimentary Basin; Geological Survey of Canada, Open File 5700, 27 p. doi:10.4095/226070

Massari, F., Ghibaudo, G., D'Alessandro, A., and Davaud, E., 2001. Water-upwelling pipes and soft-sediment-deformation structures in lower Pleistocene calcarenites (Salento, southern Italy); Geological Society of America Bulletin, v. 113, no. 5, p. 545–560. doi:10.1130/0016-7606(2001)113<0545:WUPASS>2.0.CO;2

Nichols, R.J., Sparks, R.S.J., and Wilson, C.J.N., 1994. Experimental studies of the fluidization of layered sediments and the formation of fluid escape structures; Sedimentology, v. 41, p. 233–253. doi:10.1111/j.1365-3091.1994.tb01403.x

Owen, G., 1996. Experimental soft-sediment deformation: structures formed by the liquefaction of unconsolidated sands and some ancient examples; Sedimentology, v. 43, p. 279–293. doi:10.1046/j.1365-3091.1996.d01-5.x

Park, J.K., 1994. Paleomagnetic constraints on the position of Laurentia from middle Neoproterozoic to Early Cambrian times; Precambrian Research, v. 69, p. 95–112. doi:10.1016/0301-9268(94)90081-7

Rainbird, R., 1991. Stratigraphy, sedimentology, and tectonic setting of the upper Shaler Group, Victoria Island, Northwest Territories; unpublished Ph.D. thesis, University of Western Ontario, London, Ontario, 257 p.

Rainbird, R., 1992a. Anatomy of a large-scale braid-plain quartzarenite from the Neoproterozoic Shaler Group, Victoria Island, Northwest Territories, Canada; Canadian Journal of Earth Sciences, v. 29, p. 2537–2550. doi:10.1139/e92-201

Rainbird, R., 1992b. Stratigraphy and correlation of the Neoproterozoic Shaler Supergroup, Amundsen Basin, Northwestern Canada; *in* Proceedings of the International Conference on Arctic Margins, (ed.) D.K. Thurston and K. Fujita; Anchorage, Alaska, p. 1–10.

Rainbird, R., 1993. The sedimentary record of mantle plume uplift preceding eruption of the Neoproterozoic Natkusiak flood basalt; The Journal of Geology, v. 101, no. 3, p. 305–318. doi:10.1086/648225

Rainbird, R.H., Heaman, L.M., and Young, G., 1992. Sampling Laurentia: Detrital zircon geochronology offers evidence for an extensive Neoproterozoic river system originating from the Grenville orogen; Geology, v. 20, p. 351–354. doi:10.1130/0091-7613(1992)020<0351:SLDZGO>2.3.CO;2

Rainbird, R.H., Jefferson, C.W., Hildebrand, R.S., and Worth, J.K., 1994. The Shaler Supergroup and revision of Neoproterozoic stratigraphy in Amundsen Basin, Northwest Territories; *in* Current Research 1994-C; Geological Survey of Canada, p. 61–70.

Rainbird, R.H., Jefferson, C.W., and Young, G.M., 1996. The early Neoproterozoic sedimentary Succession B of northwestern Laurentia: Correlations and paleogeographic significance; Geological Society of America Bulletin, v. 108, no. 4, p. 454–470. doi:10.1130/0016-7606(1996)108<0454:TENSSB>2.3.CO;2

Rainbird, R.H., McNicoll, V.J., Theriault, R.J., Heaman, L.M., Abbott, J.G., Long, D.G.F., and Thorkelson, D.J., 1997. Pan-continental river system draining Grenville orogen recorded by U-Pb and Sm-Nd geochronology of Neoproterozoic quartzarenites and mudrocks, northwestern Canada; The Journal of Geology, v. 105, p. 1–17. doi:10.1086/606144

Ross, J.A., Peakall, J., and Keevil, G.M., 2011. An integrated model of extrusive sand injectites in cohesionless sediments; Sedimentology, v. 58, p. 1693–1715. doi:10.1111/j.1365-3091.2011.01230.x

Sanford, B.V. and Arnott, R.W.C., 2010. Stratigraphic and structural framework of the Potsdam Group in eastern Ontario, western Quebec, and northern New York State; Geological Survey of Canada, Bulletin 597, 84 p. doi:10.4095/247669

Sweeting, M.M., 1972. Karst landforms; Macmillan Publishing Co. Ltd., London, 362 p.

Thorsteinsson, R. and Tozer, E.T., 1962. Banks, Victoria, and Stefansson Islands, Arctic Archipelago; Geological Survey of Canada, Memoir 330, 85 p.

van Loon, A.J. and Maulik, P., 2011. Abraded sand volcanoes as a tool for recognizing paleo-earthquakes, with examples from the Cisuralian Talchir Formation near Angul (Orissa, eastern India); Sedimentary Geology, v. 238, p. 145–155. doi:10.1016/j.sedgeo.2011.04.009

Washburn, A.L., 1947. Reconnaissance geology of portions of Victoria Island and adjacent regions, Arctic Canada; Geological Society of America, Memoir 22, 142 p.

Young, G.M., 1981. The Amundsen Embayment, Northwest Territories; relevance to the upper Proterozoic evolution of North America; Geological Survey of Canada, Paper 81-10, p. 203–218.

Geological Survey of Canada Project MGM 004